Journal of Magnetism and Magnetic Materials 84 (1990) 162–174
North-Holland

PHASE ANALYSIS AND MICROSTRUCTURAL CHARACTERIZATION OF $SmTiFe_{11-x}Co_x$ ($x = 0,8,11$) AND $DyTiCo_{11}$ BY TRANSMISSION ELECTRON MICROSCOPY *

S.F. CHENG, B.G. DEMCZYK, D.E. LAUGHLIN and W.E. WALLACE

Department of Metallurgical Engineering and Materials Science, Carnegie Mellon University, Pittsburgh, PA 15213, USA

Received 7 July 1989

We have examined alloys of composition $SmTiFe_{11-x}Co_x$ ($x = 0,8,11$) and $DyTiCo_{11}$ via transmission electron microscopy. Results indicate the sample without Co to be composed primarily of the body centered tetragonal 1–12 phase with a small amount of α-Fe and Fe_2Ti present. With increasing Co content, the frequency of occurrence of the 2–17 phase increases. In Sm containing samples, this phase is rhombohedral, while for Dy samples, the hexagonal phase was also found. Correspondingly, we observed an increase in the amount of transition metal-Ti solid solution as the Co concentration increases. In addition, there are orientation relationships between the 1–12 and both 2–17 phases. This is consistent with a coordinate transformation matrix based on the 1–5 structure. Both the 1–12 and 2–17 phases were found to contain antiphase boundaries in annealed samples containing Sm. The 1–12 phase alone contained antiphase boundaries in the $DyTiCo_{11}$ sample. These and other results are discussed.

1. Introduction

Among permanent magnets, the $Nd_2Fe_{14}B$ based magnets have the highest energy product (in excess of 45 MOe). However, their Curie temperatures are relatively low, leading to a large temperature coefficient of coercivity that limits the range of their application. Also, corrosion is a problem for these magnets. Therefore, there is a need to find better materials. Recently, Ohashi et al. [1] and Stadelmaier et al. [2] reported a body centered tetragonal $SmTiFe_{11}$ compound which is isomorphous with $ThMn_{12}$ (I4/mmm). This material has aroused interest due to its high room temperature anisotropy field (> 100 kOe) which renders it a promising candidate for permanent magnet applications. The Curie temperature of this material ($\approx 300\,^{\circ}C$) is comparable to that of $Nd_2Fe_{14}B$ and can be increased by replacing Fe with Co. Therefore, it is of interest to examine the effects of Co substitution on the phase distribution in the $SmTiFe_{11}$ alloy. Also, the effect of replacing Sm by other rare earth atoms (R) is of interest. In this laboratory, we have studied the magnetic properties, phase and structural characteristics in the $RTiFe_{11-x}Co_x$ system [3–9]. The results of phase analysis using scanning electron microscopy (SEM) [8] indicate the presence of a $R_2(Fe,Co,Ti)_{17}$ phase and a (Fe,Co,Ti) solid solution in addition to the $R(Fe,Co,Ti)_{12}$ phase with increasing Co content in samples annealed at 1000 °C. X-ray diffraction patterns from the 1–12 phase can be indexed based on the $ThMn_{12}$ structure. The 2–17 phase is found to have a Th_2Zn_{17} (rhombohedral) structure in light rare earth systems and generally a Th_2Ni_{17} (hexagonal) structure in systems incorporating heavy rare earths. The structural similarity of the 1–12 and 2–17 phases makes it difficult to distinguish them by X-ray diffraction, due to peak overlap. This is especially true when the amount of 2–17 phase is small. Also, the spatial resolution attainable in the SEM is not sufficient to resolve the chemical composition in fine scale multi-phase regions. Here, we will report the results of a more detailed phase and structure identification in alloys of $SmTiFe_{11-x}Co_x$ ($x = 0,8,11$) and $DyTiCo_{11}$, using both conventional (bright field/dark field imaging and selected area diffraction) and analytical (convergent beam, energy disper-

* This work was supported by grants from the Army Research Office, Research Triangle, NC, and the Materials Research Division of the National Science Foundation, Grant No. DMR-8613368.

0304-8853/90/$03.50

sive X-ray spectroscopy) transmission electron microscopy (TEM).

2. Experimental

Samples with compositions $SmTiFe_{11}$, $SmTiFe_3Co_8$ and $SmTiCo_{11}$ as well as $DyTiCo_{11}$ were prepared from high purity constituent elements by induction melting in a 450 kHz water-cooled copper boat furnace in flowing argon. Excess samarium was added to compensate for samarium loss during melting. As-cast ingots were wrapped in Ta foils, sealed in argon filled quartz tubes and annealed at 1000 °C for one week. Samples were next cut into approximately 1 mm thick sections. These were mechanically ground and polished to ≈ 40 μm. Following mounting onto 3 mm Mo rings, samples were ion beam (Ar^{2+}) milled to electron transparency. Transmission electron microscopy was performed on a Philips EM420 and a JEOL 100CX, both operating at 120 kV. The nominal probe size for convergent beam electron diffraction (CBED) and energy dispersive X-ray spectroscopy (EDXS) was ≈ 100 nm.

3. Results

3.1. General microstructure and phase identification

The $SmTiFe_{11}$ alloy has a predominantly single phase microstructure (fig. 1a), with a small amount

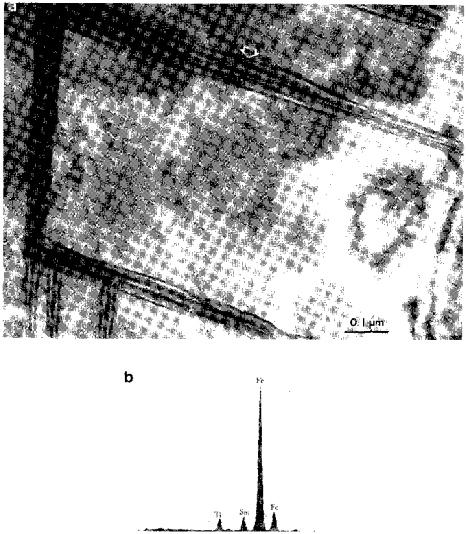

Fig. 1. (a) TEM micrograph showing single phase (1–12) $SmTiFe_{11}$. Note presence of defects exhibiting fringe contrast (arrowed); (b) corresponding EDXS spectra from the two phases.

Table 1
Phase compositions (at%) determined by energy dispersive X-ray spectroscopy

Phase	Elemental composition				
	Co	Fe	Sm	Dy	Ti
$SmTiFe_{11}$					
1–12	–	84.66	8.02	–	7.33
Fe_2Ti	–	75.1	–	–	24.9
(Fe,Ti) solid soln.	–	97.98	–	–	2.02
$SmTiFe_3Co_8$					
1–12	60.69	23.04	7.43	–	8.84
2–17	61.95	23.39	9.28	–	5.39
Solid soln.	59.48	31.49	0.85	–	8.18
$SmTiCo_{11}$					
1–12	83.82	–	7.33	–	8.84
2–7	85.39	–	9.57	–	5.03
Solid soln.	90.36	–	0.63	–	9.00
$DyTiCo_{11}$					
1–12	84.40	–	–	7.95	7.66
2–17	85.61	–	–	9.75	4.64
Solid soln.	92.73	–	–	0.12	7.15

of additional phases present. The compositions of these phases are listed in table 1. The EDXS analysis of these phases indicates that the major phase has the composition of $SmTiFe_{11}$ (fig. 1b), while the minor phases consist of nearly pure Fe and an Fe–Ti phase (table 1). A detailed analysis [10] utilizing CBED and selected area diffraction (SAD) reveals the space group of the $SmTiFe_{11}$ to be I4/mmm, which is consistent with the results of X-ray diffraction ($ThMn_{12}$ structure) [2]. Experimental measurements of higher order Laue zone (HOLZ) ring diameters using the [001] and [100] CBED patterns indicate the lattice parameters to be $a = 0.83$ nm and $c = 0.475$ nm as compared to $a = 0.856$ nm and $c = 0.479$ nm obtained from X-ray diffraction [2]. The phase containing Fe and Ti can be indexed as Fe_2Ti ($P6_3/mmc$) from its SAD patterns (e.g. fig. 2b). The amount of Ti in this phase is around 25 at% from EDXS analysis. This is slightly lower than the solubility limit (28%) for this compound expected from the binary Fe–Ti phase diagram. As mentioned above, we also observed bcc α-Fe (fig. 2a) in conjunction with the Fe_2Ti, particularly at grain boundaries. Occasionally, defects exhibiting a fringe contrast characteristic of inclined planar defects were found in the 1–12 phase (arrowed in fig. 1a). The lack of a contrast difference across the boundaries in the bright (fig. 3a) and dark (fig. 3b) images indicates that these are α fringes [11]. Fringes of this type can arise via a stacking fault, antiphase boundary (APB) or inclined planar precipitate [12]. Exten-

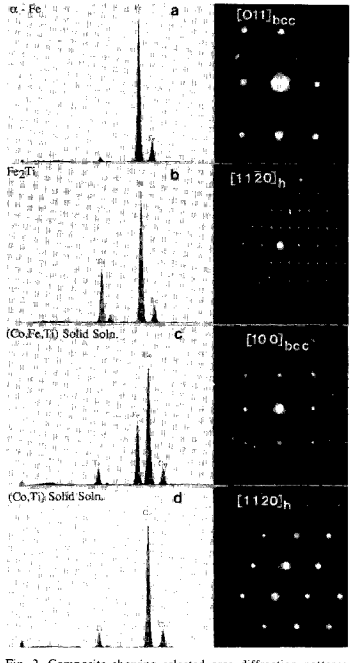

Fig. 2. Composite showing selected area diffraction patterns and corresponding EDXS spectra from observed secondary phases in $SmTiFe_{11-x}Co_x$ ($x = 0,8,11$) alloys. (a) α-Fe; (b) Fe_2Ti; (c) Co—Fe–Ti solid solution; (d) Co–Ti solid solution.

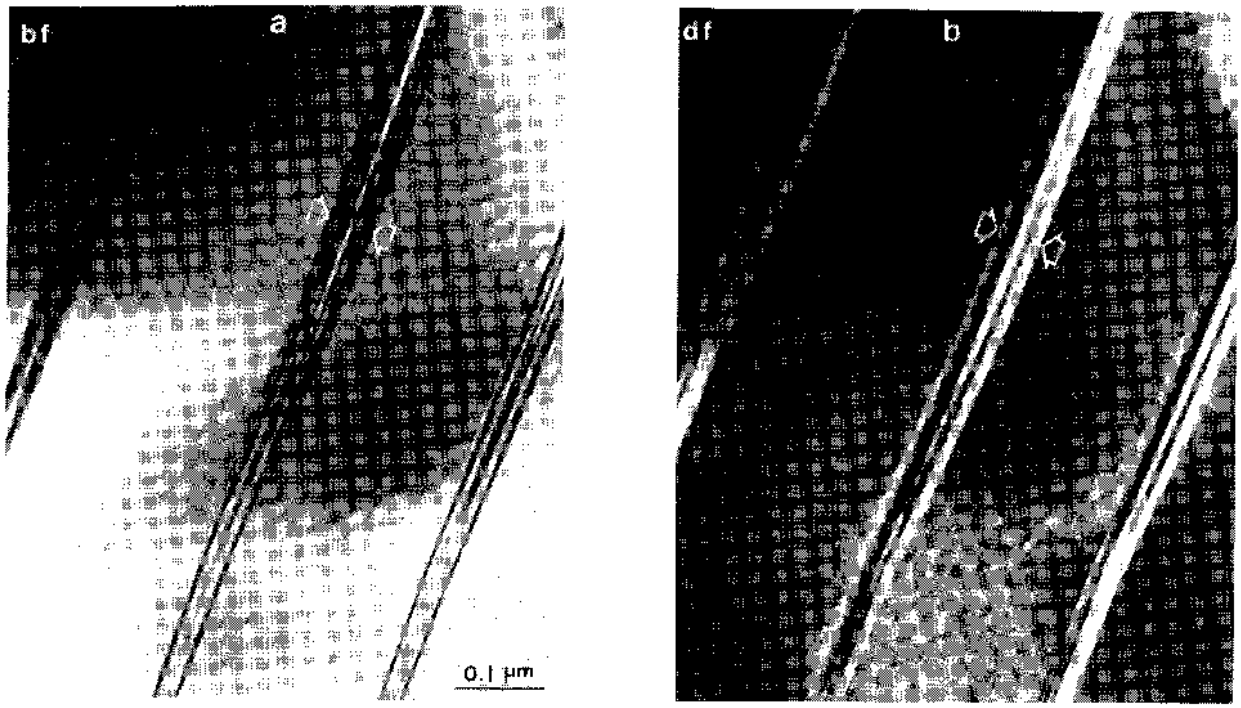

Fig. 3. (a) Bright; (b) dark field TEM images of antiphase boundaries in $SmTiFe_{11}$. Note symmetry of bounding fringes in both (a) and (b) (arrowed), and opposite nature of (a) with respect to (b).

sive trace analysis has shown these defects to lie on {100}, {110} and {101}. We have confirmed the $a/3$ [100](100) system via contrast analysis. It should be noted, however, that, due to the high density of reciprocal lattice points, it is difficult to obtain unambiguous two beam diffracting conditions, thus complicating the contrast analysis. This displacement is reasonable for an APB in light of the geometry illustrated in figs. 4a and b. Note that two different APB configurations can arise from the same displacement, depending upon from which particular atom positions the displacement is initiated. We note that, for the particular case above, the displacement vector does not lie in the antiphase plane. According to Marcinkowski [13], APBs with displacement vectors out of the anti-

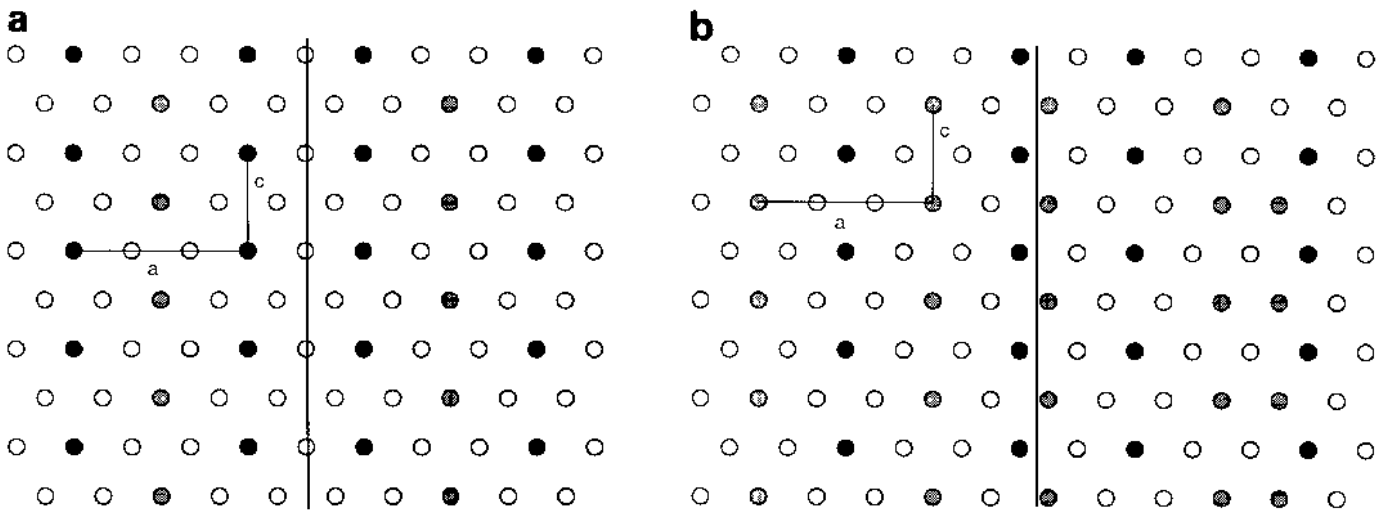

Fig. 4. (a), (b) Schematic drawing of the (010) plane of the 1–12 structure showing two possible antiphase boundary configurations generated via an $a/4$ [100](100) displacement vector. Open circles represent transition metal atoms, shaded circles rare earth atoms and solid circles, "dumbell" pairs. Note that the mean position of the dumbell pair is taken to lie in (010).

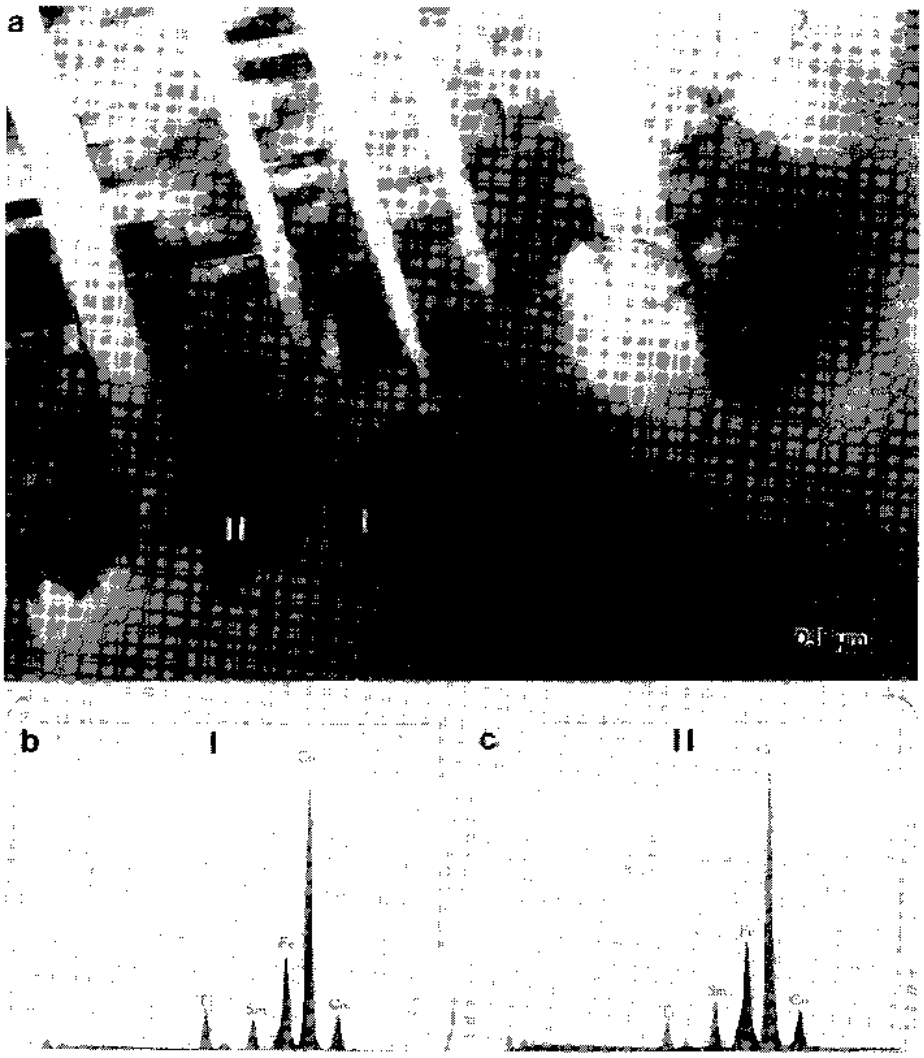

Fig. 5. (a) Micrograph of dual (1–12 and 2–17) phase region (upper) and single (1–12) phase region (lower) in $SmTiFe_3Co_8$. Note the presence of antiphase boundaries in the 2–17 phase; (b), (c) corresponding EDXS spectra from the 1–12 and 2–17 phases, respectively.

phase plane can be formed only when accompanied by the addition or removal of atoms. It is reasonable that such atom movement is facilitated by thermally assisted processes. Therefore we suggest that the antiphase boundaries observed in this phase form thermally when neighboring ordered domains grow to impingement.

Examination of $SmTiFe_3Co_8$ samples shows large single phase areas along with regions having a mixed microstructure (fig. 5a). The mixed region is seen to contain areas that exhibit numerous antiphase domains. Dark field images (figs. 6c and d) taken using individual reflections from the corresponding SAD pattern (fig. 6b) indicate the presence of two different phases in these mixed regions (fig. 6a). The results from EDXS analysis show that one phase is 1–12, while the phase which has numerous antiphase domains is 2–17 (figs. 5b and c and table 1). We observe that the 1–12 phase contains antiphase boundaries as observed in the Fe_{11} sample. Trace analysis shows that they also lie on {100}, {110} and {101}. Antiphase domain boundaries have been previously reported in the Sm_2Co_{17} phase in $SmCo_5$ alloys [14]. The preponderance of ordered domains suggests that they nucleate and grow independently from numerous sites. We will discuss ordering in 2–17 in more detail below. Besides the 1–12 and 2–17 phase, a phase containing Fe, Co and Ti was also observed (fig. 2c). This can be indexed based on bcc α-Fe, which suggests that it is a solid solution of Fe, Co and Ti. Note from

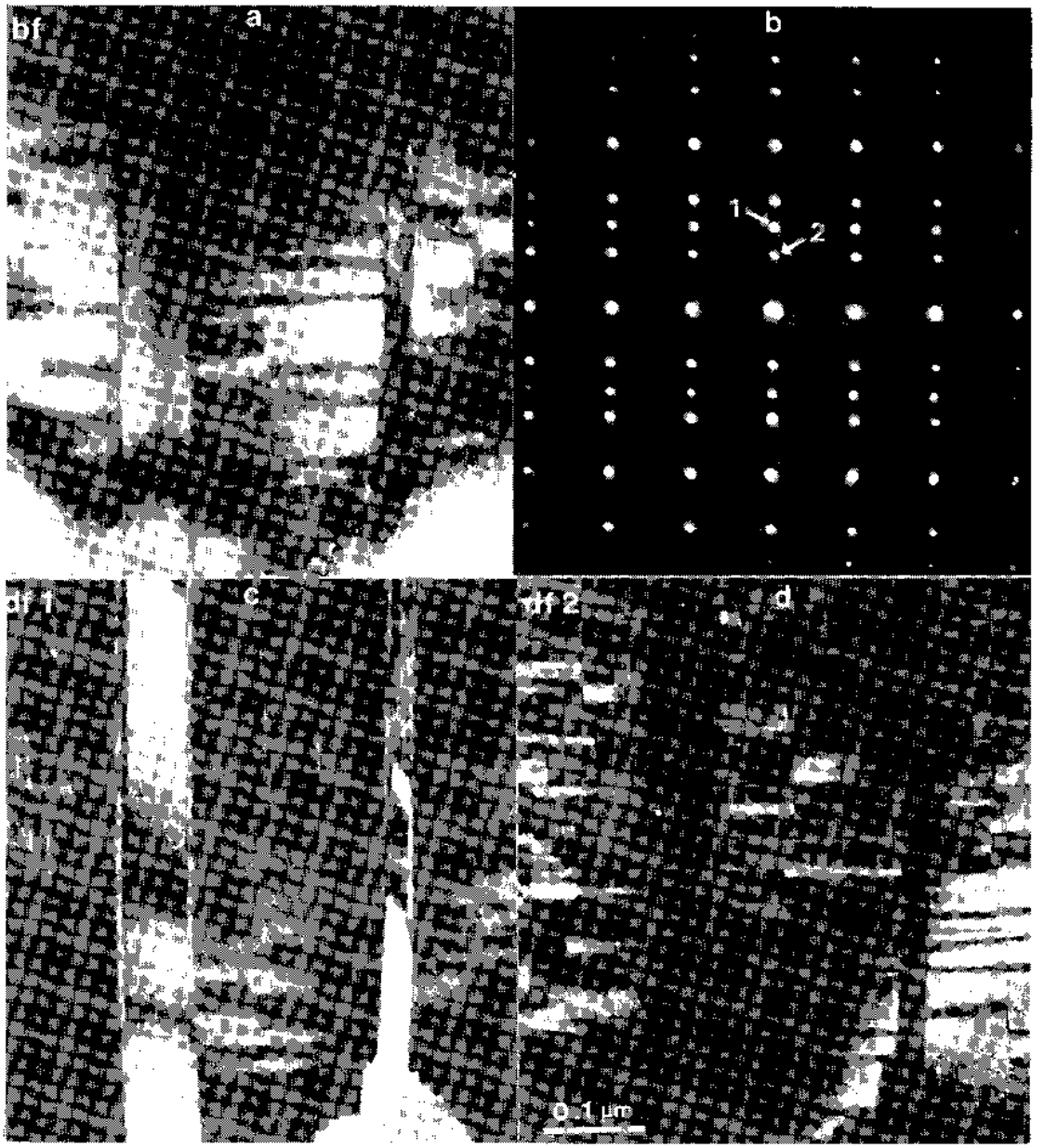

Fig. 6. (a) Bright field TEM micrograph of two phase region in $SmTiFe_3Co_8$; (b) superposed $[011]_{1-12}$ and $[1\bar{1}02]_{2-17_r}$ SAD pattern; (c), (d) dark field images taken using (c) 1–12 and (d) 2–17 diffraction spots, verifying the presence of these two phases in this region.

table 1 that this phase is Fe enriched. The Ti concentration is less than 10% in this case. The microstructure occasionally contains fine lamellae which can be identified as {112} twins from the streak direction in the SAD patterns.

Electron micrographs together with the EDXS spectra (figs. 7b and c) from the $SmTiCo_{11}$ sample show the presence of three phases, a 1–12 phase exhibiting antiphase boundaries, a mixed microstructure region (fig. 7a) containing 1–12 (labeled 1) and 2–17 (labeled 2) phases and an hexagonal (Co,Ti) solid solution (fig. 2d). The compositions of the three phases are listed in table 1. The stoichiometry of the 1–12 and 2 17 phases indicates that Fe and Co are completely miscible in these two phases. The 1–12 phase is found to possess a $ThMn_{12}$ structure, as in the Fe_{11} sample, with slight variations in lattice parameters, while the solid solution phase can be indexed based on hexagonal Co. Examination of CBED and SAD patterns from the 2–17 phase [10] indicates that the space group is $R\bar{3}m$. Measurement of both the [0001] and [1120] CBED patterns indicates the lattice parameters to be $a = 0.841$ nm and $c =$

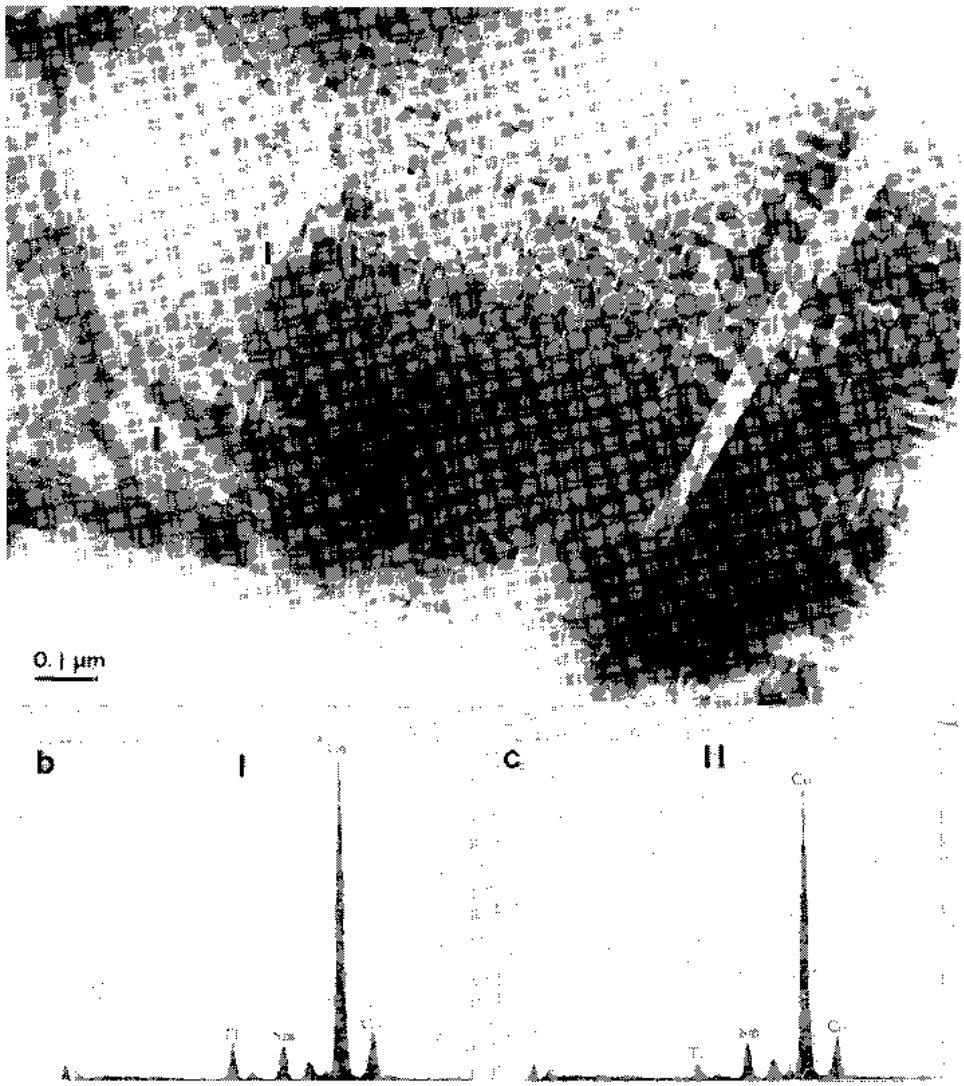

Fig. 7. (a) Bright field TEM micrograph showing the presence of two phases (1–12 (1) and 2–17 (2)) in $SmTiCo_{11}$; (b), (c) corresponding EDXS spectra from the 1–12 and 2–17 phases, respectively.

1.211 nm. This is to be compared with previous X-ray diffraction studies on binary Sm_2Co_{17}(Th_2Zn_{17} structure), which give $a = 0.842$, $c = 1.217$ nm [15]. The 2–17 phase in an as-cast $SmTiCo_{11}$ sample is also found to have the Th_2Zn_{17} structure instead of $TbCu_7$, as was found in as-cast Sm_2Co_{17} [15]. Note that the 2–17 phase contains antiphase domains present on a smaller scale than was the case for the $SmTiFe_3Co_8$ sample (compare fig. 8a with b). This suggests that the antiphase boundary energy is higher in the presence of Fe. Trace analysis on these APBs reveals that they lie primarily on $\{10\bar{1}0\}$ and $\{2\bar{1}\bar{1}0\}$ (fig. 9). We have tentatively identified the $a/3\ \langle 2\bar{1}\bar{1}0\rangle\{2\bar{1}\bar{1}0\}$ system from contrast experiments. This is illustrated schematically in figs. 10a and b. As in the 1–12 case, we see that two different APB configurations can arise from the same displacement. Thus, since the displacement vector is not in the antiphase plane, these boundaries also appear to be formed thermally. As in the $SmTiFe_3Co_8$ case, these domains are a prominent feature of the 2–17 phase microstructure. Examination of an as-cast $SmTiCo_{11}$ sample failed to reveal the presence of antiphase domains in the 2–17 phase. Also as in the $SmTiFe_3Co_8$ sample, no APBs of the type seen in the 1–12 phase were found in the 2–17 phase. We should also note that the 2–17 phase was not found in samples annealed at 1200 °C, based on concurrent SEM studies [8]. This would seem to indicate that the 2–17 phase dissolves at these temperatures and therefore that the 1–12 phase is a higher temperature phase than 2–17.

Examination of the $DyTiCo_{11}$ sample reveals a

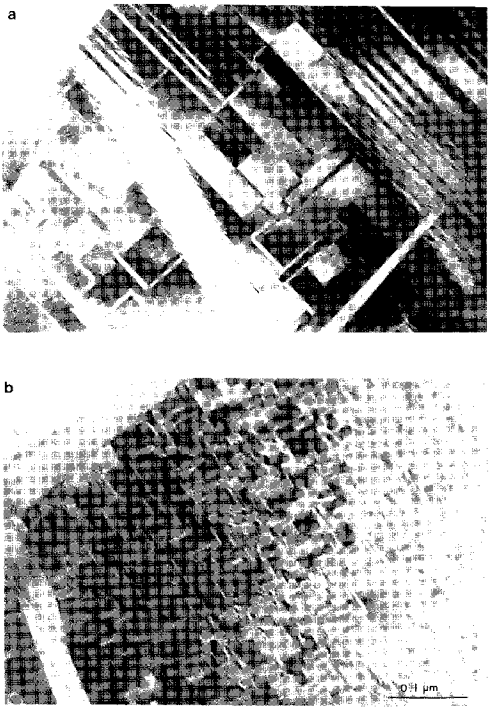

Fig. 8. Electron micrographs showing antiphase domains in 2–17 phase of (a) $SmTiFe_3Co_8$ and (b) $SmTiCo_{11}$. Note smaller domain size in (b).

similar phase distribution to $SmTiCo_{11}$. The compositions of the three observed phases are listed in table 1. CBED and SAD patterns taken from the 2–17 phase reveal the presence of an hexagonal phase as well as the rhombohedral (Th_2Zn_{17}) structure. We have determined the space group of the hexagonal phases to be $P6_3/mmc$ [10]. Experimental measurements of lattice parameters from the CBED patterns indicate $a = 0.795$ nm while $c = 0.796$ nm. The space group and the c/a ratio are consistent with results from X-ray diffraction on the hexagonal phase of binary Dy_2Co_{17} (Th_2Ni_{17} structure, $a = 0.836$, $c = 0.812$ nm) [16]. Therefore it appears that the hexagonal and

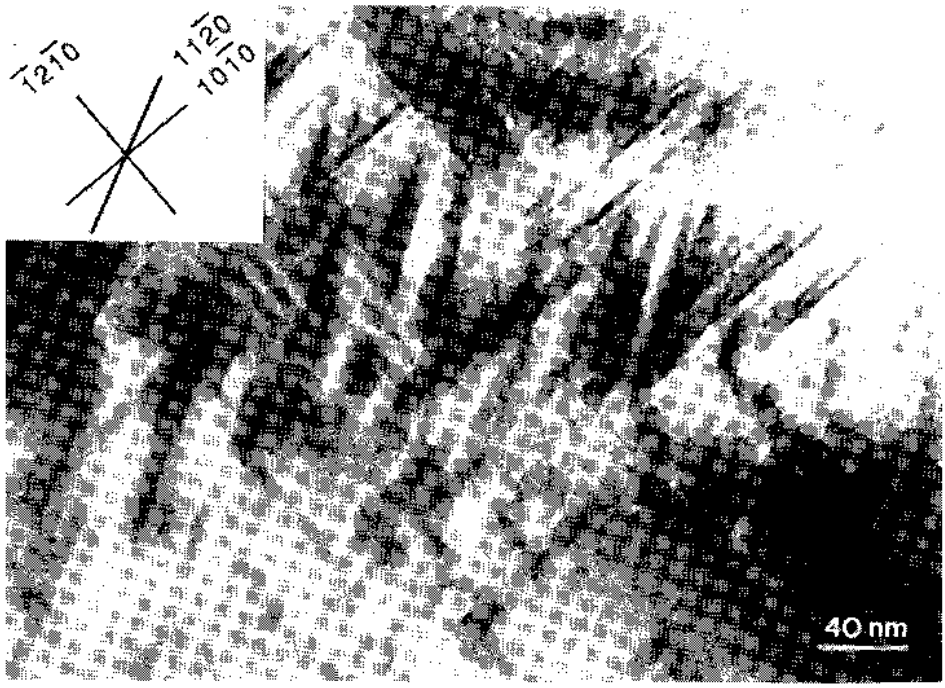

Fig. 9. TEM bright field micrographs showing antiphase boundaries in 2–17 phase of $SmTiCo_{11}$. Note from inset that the antiphase boundary traces lie close to $\{10\bar{1}0\}$ and $\{2\bar{1}\bar{1}0\}$.

rhombohedral forms of 2–17 coexist in $DyTiCo_{11}$. It is not uncommon to detect both structures within a small area, as revealed by SAD and CBED. The frequency of occurrence of the hexagonal phase seems to be much higher than the reported 50–50% distribution in binary Dy_2Co_{17} [16]. Unlike the 2–17 phase for the Sm containing samples, this hexagonal phase does not contain antiphase domains. As in the Sm case, APBs were also occasionally observed in the 1–12 phase (fig. 11).

3.2. Orientation relationships

We have observed an orientation relationship between the 1–12 tetragonal and the 2–17 rhombohedral phases in $SmTiCo_{11}$. As shown in fig. 12, this can be written as $[011]_{1-12} \| [1\bar{1}02]_{2-17}$;

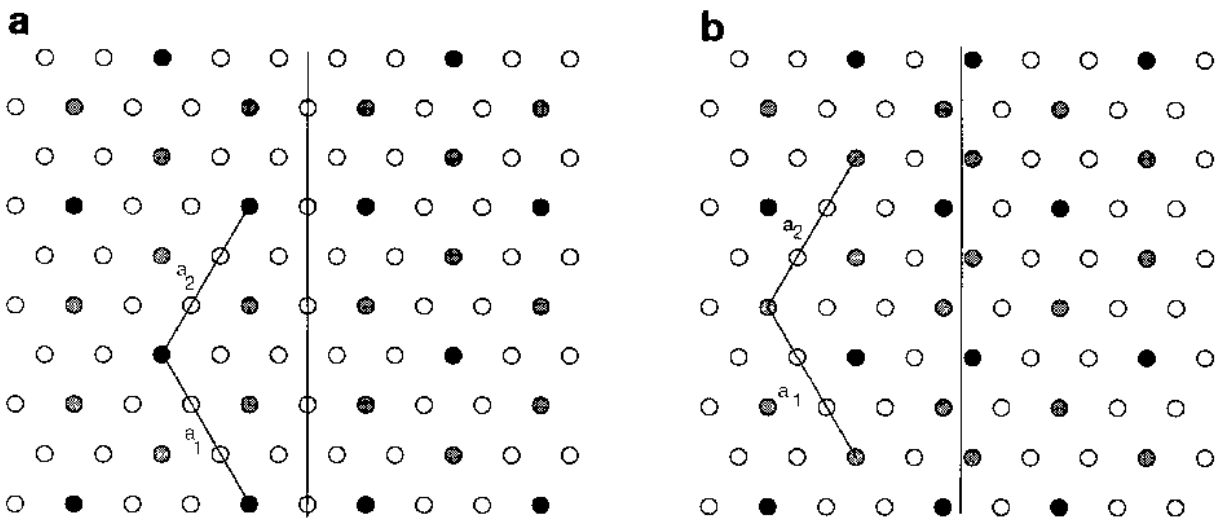

Fig. 10. Schematic drawing of the (0001) plane of the 2–17 structure showing two possible antiphase boundary configurations generated via an $a/3\ \langle 2\bar{1}\bar{1}0\rangle\{2\bar{1}\bar{1}0\}$ displacement vector. Open circles represent transition metal atoms, shaded circles, rare earth atoms and solid circles, "dumbell" pairs. Note that the mean position of the dumbell pairs is taken to lie in (0001).

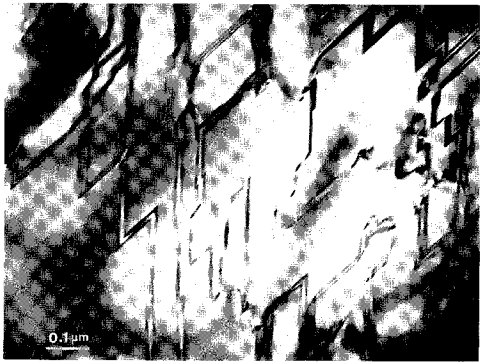

Fig. 11. Electron micrograph showing antiphase domain boundaries observed in 1–12 phase of $DyTiCo_{11}$.

$(200)_{1-12}\|(11\bar{2}0)_{2-17}$. A similar relationship (written as $[123]_{1-12}\|[2\bar{1}\bar{1}3]_{2-17}$; $(30\bar{1})_{1-12}\|(0110)_{2-17}$ in fig. 13) was found between the 1–12 tetragonal and 2–17 hexagonal phases in $DyTiCo_{11}$. Such a relationship is possible since both the 1–12 and 2–17 phases are structural derivatives of the hexagonal 1–5 structure, as described in ref. [17]. The general formula of 1–5 derivatives in rare earth transition metal systems can be written as $R_{m-n}T_{5m-2n}$, where R is a rare earth atom; T, a transition metal atom; m, the number of 1–5 unit cells; and n, the number of R atoms being replaced by T metal pairs. Table 2 shows the values of m and n as well as the relationship of the lattice parameters for these phases in their idealized structures. The crystallographic relationship between these phases is shown in fig. 14 which is a view looking onto the (0001) plane of the 1–5 (and 2–17) structure and the (010) plane of the 1–12 structure. Note that the $2\text{–}17_r$ is referred to hexagonal axes. From fig. 14 and table 2 we can derive the following coordinate transformation matrices

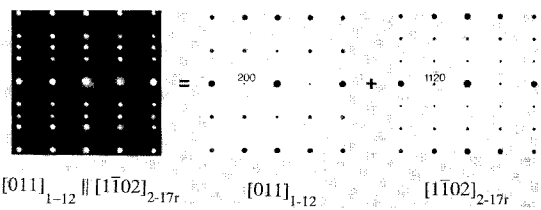

Fig. 12. Composite selected area diffraction pattern from two phase region in $SmTiCo_{11}$, along with computed $[011]_{1-12}$ and $[1\bar{1}02]_{2-17_r}$ SAD patterns illustrating the orientation relationship between these phases. Note additional spots in patterns arising from double diffraction.

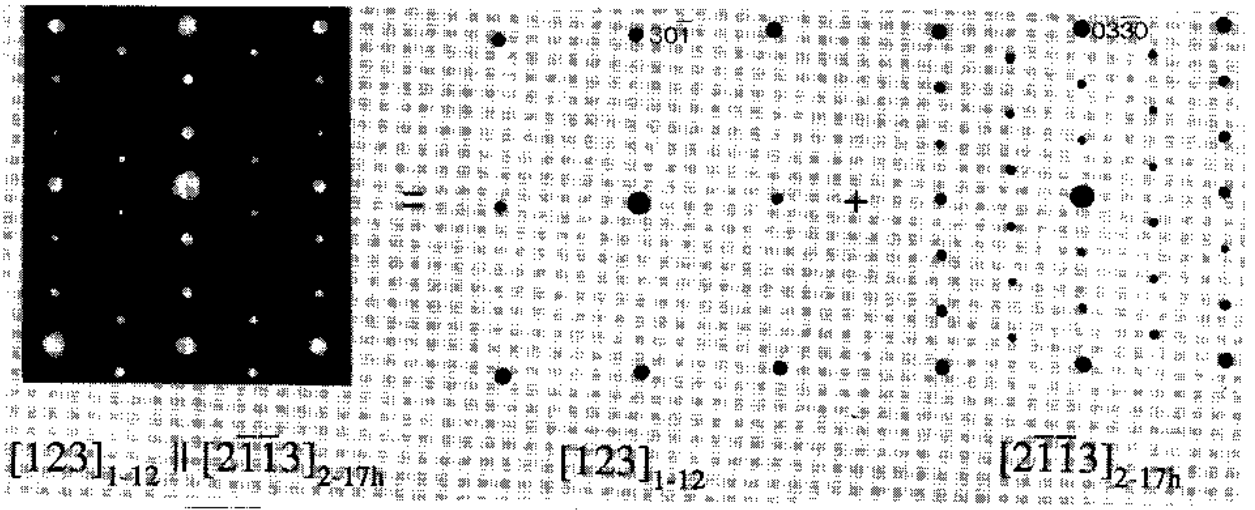

Fig. 13. Composite selected area diffraction pattern across phase boundary in $DyTiCo_{11}$, along with computed $[123]_{1-12}$ and $[2\bar{1}\bar{1}3]_{2-17_h}$ SAD patterns illustrating the orientation relationship between these two phases.

Table 2
Phase stoichiometry and phase relationships (refer to text for details)

Phase	Crystal system	m	n	a'	b'	c'
1– 5	hexagonal	1	0	a	a	c
2–17	hexagonal	6	2	$\sqrt{3}a$	$\sqrt{3}a$	$2c$
2–17	rhombohedral	9	3	$\sqrt{3}a$	$\sqrt{3}a$	$3c$
1–12	tetragonal	4	2	$\sqrt{3}a$	$\sqrt{3}a$	a

Key: $R_{m-n}T_{5m+2n}$ = the general formula for 1–5 and its T-rich derivatives, where:
R = a rare earth atom, T = a transition metal atom, m = the number of 1–5 unit cells, n = the number of R atoms being replaced by T metal pairs.

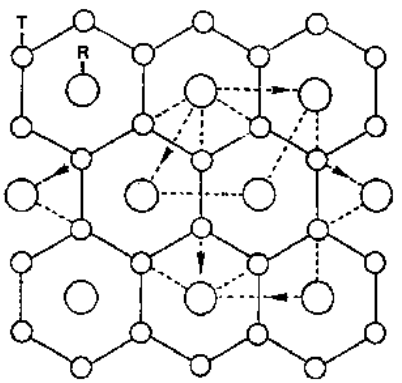

Fig. 14. Schematic drawing of the (0001) plane of 1–5 (and 2–17) and the (010) plane of 1–12. In the drawing, the small and large rhombi represent the 1–5 and 2–17 cells, respectively, and the rectangle, the 1–12 cell. In the latter case, the longer dimension is a and the smaller, c.

between the 1–12 and 2–17 hexagonal and the 1–12 and 2–17 rhombohedral phases:

$$(HKL)_{1-12} = (hkl)_{2-17_h}\begin{pmatrix} 1 & 0 & 1/3 \\ 1 & 0 & -1/3 \\ 0 & 1 & 0 \end{pmatrix},$$

$$\begin{pmatrix} U \\ V \\ W \end{pmatrix}_{1-12} = \begin{pmatrix} 1/2 & 1/2 & 0 \\ 0 & 0 & 1 \\ 3/2 & -3/2 & 0 \end{pmatrix}\begin{pmatrix} u \\ v \\ w \end{pmatrix}_{2-17_h};$$

$$(HKL)_{1-12} = (hkl)_{2-17_r}\begin{pmatrix} 1 & 0 & 1/3 \\ 1 & 0 & -1/3 \\ 0 & 2/3 & 0 \end{pmatrix},$$

$$\begin{pmatrix} U \\ V \\ W \end{pmatrix}_{1-12} = \begin{pmatrix} 1/2 & 1/2 & 0 \\ 0 & 0 & 3/2 \\ 3/2 & -3/2 & 0 \end{pmatrix}\begin{pmatrix} u \\ v \\ w \end{pmatrix}_{2-17_r}.$$

Note that the Miller indices were used for the 2–17 system. The observation of the orientation relationships is consistent with the above transformation matrices.

4. Discussion

Experimental results indicate that the 2–17 phase in both as-cast and annealed samples possesses a Th_2Zn_{17} structure. As reported above, we observed numerous antiphase domains in the

rhombohedral 2–17 phase in annealed $SmTiFe_3Co_8$ and $SmTiCo_{11}$ samples. The 2–17 phase in the as-cast state was not found to contain APBs. Since the antiphase domain boundaries can be formed as a result of the transformation from disorder to order, it is suggested that the 2–17 phase orders during annealing. This transformation proceeds first by the nucleation of small ordered regions. These regions grow to impingement, forming antiphase domain boundaries. As noted above, it was experimentally observed that the APB displacement vector lies out of the APB plane. This, along with the preponderance of individual ordered domains in these materials supports thermally assisted formation process.

Ray [18] has reported a disordered Th_2Zn_{17} structure in solutionized and quenched 2–17 type magnets. He suggested that, in the disordered structure, the dumbell sites are randomly occupied by different atoms. After aging, these dumbell sites are preferentially occupied by Zr-vacancy pairs, resulting in an ordered Th_2Zn_{17} structure. We propose a similar scenario in the present case, involving Ti–Co pairs instead of the Zr-vacancy pairs mentioned above (i.e. the dumbell sites are preferentially occupied by Ti–Co pairs (see below)). It is generally believed that one reason for the formation of a cellular structure in 2–17 type magnets is the stability of different elements in different phases (e.g. Fe prefers to enter the 2–17 phase and Cu the 1–5 phase). Therefore, even in nearly stoichiometric 2–17 alloys (e.g. $Sm(Co_{0.65}Fe_{0.25}Cu_{0.08}Zr_{0.02})_{8.35}$), a cellular structure is observed [19]. That is, the ordered domains of the 2–17 phase are prevented from growing to impingement by the presence of the 1–5 phase, which surrounds the ordered 2–17 regions. Thus no APBs are observed. The domain size in our $SmTiFe_3Co_8$ samples is on the order of 0.05 μm, which is comparable with the observed cell size in 2–17 magnets (of course, these are both composition and heat treatment dependent). Since, in our system, Fe and Co atoms are completely miscible in the 2–17 phase and since there are no additional elements (e.g. Cu) present to induce phase separation, there is no tendency to form a second (e.g. 1–5) phase. This may explain why the microstructure resulting from the phase transformation from disordered-to-ordered 2–17 consists of antiphase domains rather than a cellular structure. The lack of APBs in the hexagonal 2–17 phase of the $DyTiCo_{11}$ sample is possible since the two commonly observed "Th_2Ni_{17}" prototype structures ($P6_3/mmc$ or $P6/mmm$) are partially disordered due to the additional random substitution of T–T pairs at rare earth sites [20]. As in the rhombohedral 2–17 case, trace and contrast analysis of APBs in the 1–12 phase suggests that their formation also requires atom removal. Since the 1–12 and 2–17 structures are similar (both being derivatives of 1–5) and the displacement systems were found to be analogous in both structures (fig. 4), it is reasonable that the ordering in these two phases is similar (i.e. preferential dumbell occupancy).

As mentioned in the discussion of the orientation relationships, the general formula of the 1–12 and 2–17 phases can be written as $R_{m-n}T_{5m+2n}$. Alternatively, we can write this as $R_{m-n}T_{5m}T'_{2n}$, where T′ is the type (or types) of atom(s) occupying the dumbell positions. For our samples, R is Sm or Dy and T is Fe and/or Co. From the m and n values listed in table 2, the formula of the 1–12 phase is $R_2T_{20}T'_4$ while the 2–17 phases are $R_4T_{30}T'_4$ and $R_6T_{45}T'_6$ for the hexagonal and rhombohedral forms, respectively. If the dumbell is comprised of Ti–Ti pairs (i.e. T′ = Ti), the R/Ti ratio will be 0.5 for the 1–12 phase and 1 for both the hexagonal and rhombohedral forms of the 2–17 phase. Our EDXS analyses show that the R/Ti ratio in the 1–12 phase is nearly 1, while in both forms of the 2–17 phase, it is nearly 2. This suggests that the dumbells are made up of either Ti–Ti or Ti–vacancy instead of Ti–Ti pairs and that the Ti atoms occupy the dumbell sites preferentially in all three phases. This is reasonable in light of atomic size consideration (Ti is ≈ 17% larger than either Fe or Co). Neutron diffraction studies of $YTiFe_{11}$($ThMn_{12}$ structure) [21] indicate that the 2a sites are occupied by Y, the 8i sites by both Ti and Fe atoms and the 8j and 8f sites by Fe alone. Since dumbell sites are associated with the i sites, this is consistent with our assumption that the dumbell sites are occupied by Ti–T pairs. Furthermore, Satyanarayana et al. [22] have shown the preferential substitution

of dumbell Co atoms by Ti in rhombohedral Sm_2Co_{17}, based on the observed increase of the anisotropy field and the c/a ratio as Co is replaced by Ti. If Ti–vacancy pairs substitute for Co–Co pairs, the c/a ratio would be expected to decrease. Also, Ti–Ti substitution is highly unlikely due to atomic size considerations. This further supports our contention regarding Ti–T pair substitution in the dumbell sites. Thus it is reasonable to assume that the ordered state consists of dumbells composed of Ti–T pairs.

5. Summary

We have examined alloys of the composition $SmTiFe_{11}$, $SmTiFe_3Co_8$, $SmTiCo_{11}$ and $DyTiCo_{11}$. Results indicate the Sm-containing $TiFe_{11}$ sample to be composed primarily of the body centered tetragonal 1–12 phase (space group I4/mmm) with additional Fe_2Ti and α-Fe phases present. The Fe_3Co_8 sample is composed of rhombohedral 2–17 phase ($R\bar{3}m$) and bcc Co–Fe–Ti solid solution in addition to the 1–12 phase. In $SmTiCo_{11}$, all three phases are observed. In this case, however, the solid solution phase can be indexed (based on Co) as hexagonal. When Dy is substituted for Sm in the Co_{11} sample, the hexagonal 2–17 phase (space group P63/mmc) was found in addition to the rhombohedral phase. We observed an orientation relationship between both the 1–12 and 2–17 rhombohedral and 1–12 and 2–17 hexagonal phases. Antiphase boundaries were found in the 1–12 phase as well as the rhombohedral 2–17 phase in annealed samples containing Sm. Trace and contrast analysis seems to indicate that these are formed thermally. It is proposed that these phases order when the dumbells are comprised of Ti–T pairs.

References

[1] K. Ohashi, Y. Tawara, R. Osugi, J. Sakurai and Y. Komura, J. Less-Common Met. 139 (1988) L1.
[2] H.H. Stadelmaier, F.J. Cadieu and N.C. Liu, Mater. Lett. 6 (1988) 80.
[3] S.F. Cheng, V.K. Sinha, Y.Xu, J.M. Elbicki, W.E. Laughlin, S.G. Sankar and D.E. Laughlin, J. Magn. Magn. Mat. 75 (1988) 330.
[4] E.B. Boltich, B.M. Ma, L.Y. Zhang, F. Pouranian, S.K. Malik, S.G. Sankar and W.E. Wallace, J. Magn. Magn. Mat. 78 (1989) 364.
[5] V.K. Sinha, S.K. Malik, D.T. Adroja, J.M. Elbicki, S.G. Sankar and W.E. Wallace, J. Magn. Magn. Mat. 80 (1989) 281.
[6] L.Y. Zhang, E.B. Boltich, V.K. Sinha and W.E. Wallace, Proc. Intermag. Conf., March 1989, IEEE Trans. Magn. (1989) in press.
[7] V.K. Sinha, S.F. Cheng, W.E. Wallace and S.G. Sankar, J. Magn. Magn. Mat. 81 (1989) 227.
[8] S.F. Cheng, V.K. Sinha, B.G. Demczyk, W.E. Wallace and D.E. Laughlin, unpublished research.
[9] S.F. Cheng, V.K. Sinha, Y. Xu and W.E. Wallace, J. Magn. Magn. Mat. (to be submitted).
[10] B.G. Demczyk, S.E. Cheng and D.E. Laughlin, unpublished research.
[11] S. Amelinckx and J. Van Landuyt, in: Diffraction and Imaging Techniques in Materials Science, eds. S. Amelinckx, R. Gevers and J. Van Landuyt (North-Holland, Amsterdam, 1978) p. 107.
[12] J.W. Edington, Practical Electron Microscopy in Materials Science (Van Nostrand Reinhold, New York, 1976) p. 206.
[13] M.J. Marcinkowski, in: Electron Microscopy and Strength of Crystals, eds. G. Thomas and J. Washburn (Wiley–Interscience, New York, 1963) p. 333.
[14] P. Rao, J.G. Smeggil and E.F. Koch, Proc. 31st EMSA (Claitor's Publ. Div., Baton Rouge, 1973) p. 186.
[15] W. Ostertag and K.J. Strnat, Acta Cryst. 21 (1966) 560.
[16] Y. Kahn, Acta Cryst. B 29 (1973) 2502.
[17] H.H. Stadelmaier, Z. Metallk. 75 (1984) 227.
[18] A.E. Ray, J. Appl. Phys. 55 (1984) 2094.
[19] A.E. Ray, IEEE Trans. Magn. MAG-20 (1984) 1614.
[20] A.E. Ray, in: Soft and Hard Magnetic Materials with Applications, ed. J.A. Salsgiver (Am. Soc. for Metals, Metals Park, OH, 1986) p. 105.
[21] O. Moze, L. Pareti and M. Solzi, Solid State Commun. 66 (1988) 465.
[22] M.V. Satyanarayana, H. Fujii and W.E. Wallace, J. Appl. Phys. 53 (1982) 2374.